

## Experimental and analytical investigations for behaviors of RC beams strengthened with tapered CFRPs

Naeun Kim, Young Hee Kim and Hee Sun Kim\*

Department of Architectural Engineering, Ewha Womans University,  
52, Ewhayeodae-gil, Seodaemun-gu, Seoul 120-750, Republic of Korea

(Received September 8, 2013, Revised August 25, 2014, Accepted October 9, 2014)

**Abstract.** This study investigates structural and mechanical behaviors of RC (Reinforced concrete) beams strengthened with tapered CFRP (Carbon fiber reinforced polymer) sheets having various configurations. Toward this goal, experiments are performed on RC beams strengthened with four layers of CFRP sheets and each layer of the CFRP is prepared to have different length. Experimental results show that tapered CFRPs have better strengthening effect than non-tapered CFRP sheets and maximum loads of the beams with tapered CFRPs are governed by the length of first CFRP layer rather than total length of CFRP layers. In addition, analyses are performed using FE (Finite Element) models including cohesive elements to predict debonding behaviors between FRP and concrete elements. The predicted results from the FE models show good agreement with the experimental results.

**Keywords:** Finite Element Method (FEM); fiber reinforced; composites; analytical method; experimental investigation

---

### 1. Introduction

CFRP (Carbon fiber reinforced polymer) sheets have been widely used to strengthen concrete structures. Especially, flexural strength of RC (Reinforced concrete) beams can be significantly improved when CFRP sheets are externally attached to bottom surface of the beams. Among various influencing parameters on structural behaviors of RC beams strengthened with CFRP sheets or plates, length, thickness, and width of FRP sheets or plates are the most critical factors to determine strengthening effect. Generally, it is recommended to use FRP sheets longer than the effective bond length and ACI repair manual (2008) suggests an equation for effective bond length of FRP sheets. There are researchers proposing equations for effective bond length, e.g., Mongi *et al.* (2009) suggest that the effective bond length is proportional to the stiffness of the FRP. Regarding the length of FRP plate, Al-Tamimi *et al.* (2011) have found that strengthening effect of RC beams depends on CFRP plate length/shear span ratio and Hawileh *et al.* (2013) develop FE modeling methods to predict behaviors of RC beams strengthened with short-length CFRP plates. Meanwhile, it is reported that there is no significant effect of the CFRP length on structural

---

\*Corresponding author, Assistant Professor, E-mail: [hskim3@ewha.ac.kr](mailto:hskim3@ewha.ac.kr)

<sup>a</sup>Graduate Student

behavior, when the length of FRP is larger than 60% of the span length of the high strength concrete continuous beams (Kadhim 2011). In addition, Gao *et al.* (2006) perform experiments on RC beams with tapered CFRP sheets, and find that tapered CFRP sheets can enhance the strengthening effect and load carrying capacity, compared with RC beams strengthened with non-tapered CFRP sheets. Relationships between debonding and CFRPs thickness are experimentally investigated by Leung (2006). Also, Maalej and Leong (2005) perform experiments to show relationships between CFRPs thickness and interfacial stress, and conclude that interfacial stress increases with the number of CFRP layers. The effect of the CFRPs width on the structural behavior of RC beams is also investigated by Brena and Macri (2004).

Also, some of the existing researches are focused on investigation of the debonding behaviors of CFRP sheets, mainly because premature and sudden failures due to the debonding of CFRP sheets is one of the common failure modes for the case of RC (reinforced concrete) beams strengthened with CFRP sheets (Kang *et al.* 2012, Teng *et al.* 2001). In order to predict such behaviors analytically, Smith and Teng (2002) introduce analytical modeling approaches for the bonding strength of RC beams strengthened with CFRPs. Yang *et al.* (2002) and Teng *et al.* (2006) develop analytical methods to predict interfacial stress between concrete and CFRPs. To predict the debonding behavior, Camata *et al.* (2007) propose a model using a smeared and interfacial crack model that includes actual crack patterns observed from loading tests of RC beams flexurally strengthened with CFRPs. In addition, Obaidat *et al.* (2010) perform finite element analysis to predict the behavior of RC beams strengthened with CFRPs and show the significance of modeling the debonding characteristics for better prediction.

In this study, experimental and analytical studies are performed to evaluate the structural and mechanical behaviors of RC beams externally strengthened with tapered CFRP sheets. For the experiments, RC beams are strengthened with four layers of CFRP sheets having different lengths of CFRP per layer and subjected to four point-bending with the simply supported condition. In order to examine the strengthening effect of CFRP length and the termination point of each CFRP layer, maximum loads, deflections, and strains of CFRP, reinforcing steel bars and concrete are obtained from the experiments. In addition, analytical models are generated including cohesive elements for epoxy to verify the structural behavior of RC beams with tapered CFRPs.

## 2. Experimental and analytical program

### 2.1 Experimental approach

#### 2.1.1 Details of tested beams

For testing, five RC beams with the dimensions of 200×250×3200 mm (width×depth×length) are fabricated and mixture ratios for the concrete are listed in Table 1. After 28 days of concrete pouring, compressive and tensile strengths of the concrete are measured as 29 MPa and 3 MPa, respectively. All beams use reinforcing steel bars of two deformed bars with diameter of 13 mm in tensile section and stirrups with diameter of 10 mm at 100 mm intervals. Details of the beams including configurations of tapered CFRP sheets are illustrated in Figs. 1(a)-(e). For tapered CFRP sheets, the length of each CFRP layer is prepared as listed in Table 2. Specimen CONT is a control specimen that is reinforced with steel bars only, whereas specimens 4A, 4B, 4C, and 4D are strengthened with four layered CFRP sheets. Specimen 4A is strengthened with the same length of CFRPs, while specimens 4B, 4C and 4D have tapered CFRPs such that the length of the CFRP

Table 1 Mix proportions for concrete

Compressive strength	W/C (%)	s/a (%)	Weight per unit volume (kg/m <sup>3</sup> )				
			W	C	S	G	AD
29MPa	44.2	46.9	165	373	837	966	1.87

W : Water  
 C : Cement  
 S : Sand  
 G : Coarse aggregate  
 AD : Admixture

Table 2 List of specimens

Specimen	CFRP length (mm)			
	1 <sup>st</sup> layer	2 <sup>nd</sup> layer	3 <sup>rd</sup> layer	4 <sup>th</sup> layer
4A	1800	1800	1800	1800
4B	1800	1500	1200	900
4C	2100	1800	1500	1200
4D	2400	2100	1800	900

layer becomes shorter than the previously attached CFRP layer. Differences among 4B, 4C, and 4D can be found from the length of CFRP layer attached directly to the concrete beam surface; however the total lengths of CFRP used in specimens 4B and 4D are controlled to be the same. ACI code (2008) suggests an equation for the effective bond length as shown in Eq. (1), where n is number of FRP sheets,  $E_f$  and  $t_f$  are elastic modulus and thickness of FRP sheets, respectively. Based on this equation, the effective bond length is 640mm for strengthening RC beams when strengthened with four layers of FRP sheets. Therefore, the lengths of CFRPs used in this study satisfy the effective bond length according to ACI code (2009). Also, the widths of CFRPs are equal to the width of the concrete beams.

$$L_e = \frac{23300}{(nE_f t_f)^{0.58}} \tag{1}$$

$n$ : number of FRP sheets,  $E_f$ : elastic modulus of FRP sheets,  $t_f$ : thickness of FRP sheets

### 2.1.2 FRP bonding and fabrication of specimens

The CFRP sheets provided by Hankuk Carbon (Hankuk Carbon, Co.) are used for strengthening the RC beams. The full process of reinforcement by CFRP sheets is performed according to the following steps under the manufacturer’s supervision: 1) Bottom surfaces of the concrete beams are ground smooth using a mechanical grinder to remove the surface laitance, grease, and debris. 2) Remaining dust and free particles on the concrete surface are vacuum-cleaned after the grinding works. 3) The ground RC beam surfaces are then thinly coated with primer, which penetrates into the concrete substrates and results in a denser concrete surface. After primer coating, adhesive is applied on the surfaces of the beams. 4) The CFRP sheets are cut in a parallel direction to the fiber directions and impregnated with the adhesives before being attached to the beams. 5) The CFRPs attached to the beams are cured under room temperature for 7 days.

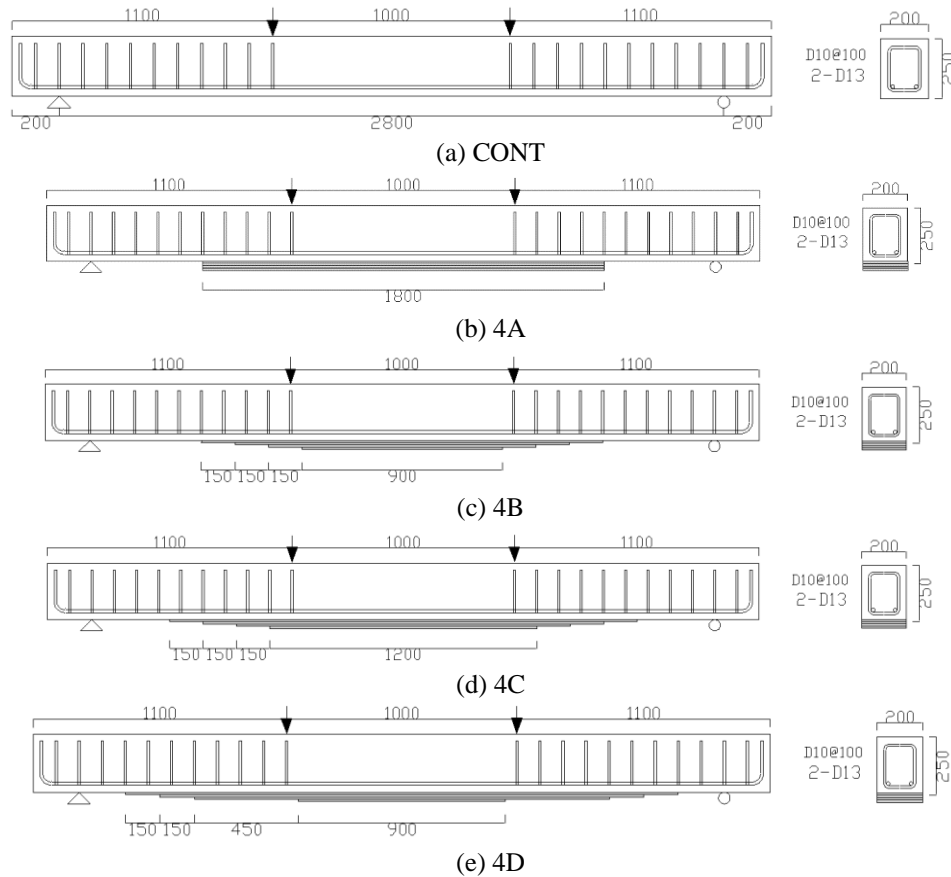


Fig. 1 Detail of specimens

Table 3 Material properties of CFRPs and adhesives

Type	Thickness (mm)	Elastic modulus (GPa)	Tensile strength (MPa)	Flexural strength (MPa)
CFRP	0.5	245.2	4500	-
Primer	3.2	2.46	55	82.4
Top-coat	3.2	3.11	63	99.3

The material properties of the CFRPs and the adhesive are also provided from the manufacturer as shown in Table 3.

### 2.1.3 Instrumentation and testing

After curing, the fabricated beams are subjected to four-point bending with an effective span of 2800mm as illustrated in Fig. 2. A universal testing machine of 500kN is used to apply loads in a displacement control with a loading rate of 4 mm/min. During testing, vertical deflections of the beams are measured by linear variable differential transformers (LVDTs) located at mid-span and the quarter points of the effective span from the supports. Strains of concrete are monitored using

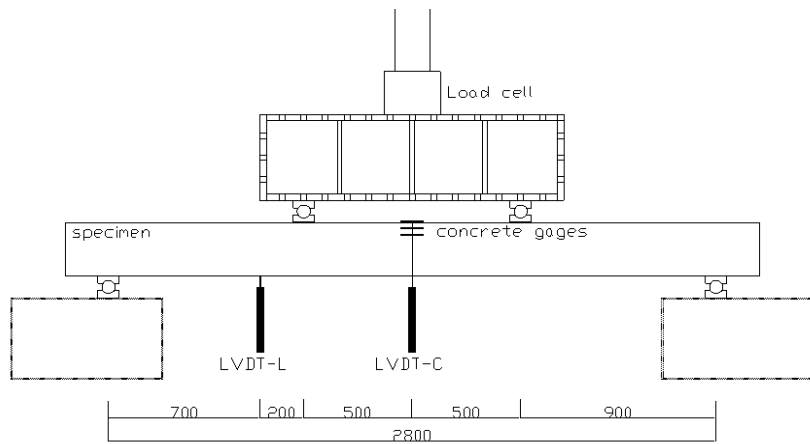
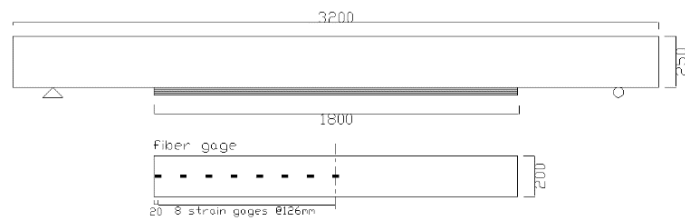
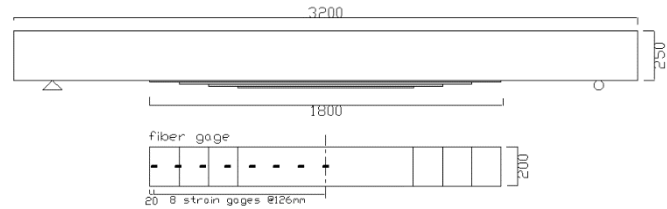


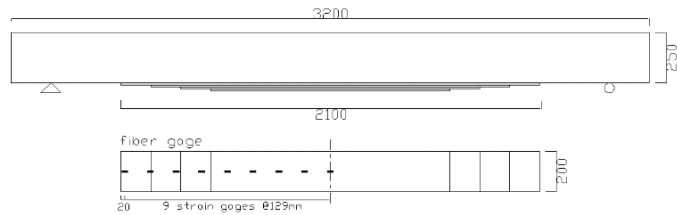
Fig. 2 Test set-up and instrumentation



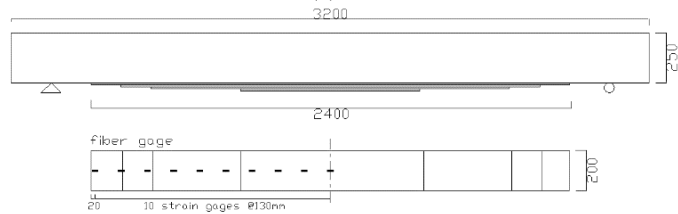
(a) 4A



(b) 4B



(c) 4C



(d) 4D

Fig. 3 Location of strain gages on CFRPs

three strain gauges attached on the top and side surfaces of the beams with 30mm intervals as illustrated in Fig. 2. In order to calculate interfacial shear stresses between the concrete beams and CFRP sheets, multiple strain gauges are attached on the CFRP sheets with intervals of 126-130 mm as shown in Figs. 3(a)-(d).

## 2.2 Finite element modeling approach

FE (Finite element) analyses of the RC beams strengthened with various configurations of CFRPs are performed using the commercial FE software, ABAQUS version 6.10-3 (ABAQUS, 2010). As illustrated in Fig. 4, the FE model consists of four parts, namely concrete, steel, epoxy, and CFRPs, and each part is modeled using different element type and elastic modulus as presented in Table 4. Concrete and steel reinforcement are generated using 3D continuum brick elements and 3D truss elements, respectively. Instead of generating half model based on symmetrical plane, full models are generated due to relatively short computational time. To consider material nonlinearity, existing experimental data obtained from compressive and tensile material tests of concrete and steel bars are adopted. For epoxy, cohesive elements are used with elastic-traction material behavior to consider debonding (Choi *et al.* 2013). In the epoxy model, a damage initiation criterion is also included to consider debonding. The criteria for debonding initiation is obtained from the previous study (Choi *et al.* 2013), where tests results of small sized concrete beams strengthened with FRP sheets are reported. In this manner, the FE model is able to debonding of CFRP sheets caused by stresses of epoxy. For CFRPs, shell elements are used with a linear elastic material model considering fiber direction. Between the CFRP sheets, perfect bonding is assumed because delamination between the CFRP sheets is not observed from the experiments. The loading is prescribed in a form of displacement control and the analytical procedure includes geometrical nonlinearity to increase the degree of accuracy.

## 3. Results and discussion

### 3.1 Experimental results

#### 3.1.1 Load-deflection relationships

Load-deflection curves obtained from the experiments are illustrated in Fig. 5. For the control beam, load-deflection curve shows a long plateau in regions of plastic behaviors, while the stiffer slope and sudden termination of the load-deflection curves are shown for the beams strengthened with CFRPs. Commonly, maximum loads of beams with CFRPs are about 1.2-2.0 times higher than the maximum load of the control beam and deflections of beams with CFRPs at failure are about 0.14-0.36 times smaller than the deflection of the control beam. Among the beams strengthened with CFRPs, 4A shows the lowest maximum loads and the earliest failure. The reason for showing the lowest maximum load with the earliest failure in specimen 4A is that the stresses are highly concentrated at the end of the CFRPs as the length of each CFRP layer is the same as 1800 mm. In other words, the beams strengthened with tapered CFRPs show higher load capacities than the beam strengthened with non-tapered CFRPs, because tapered CFRP is able to reduce stress concentration at the end of FRP sheets. Even though total length and axial stiffness (elastic modulus $\times$ thickness of CFRPs) of CFRPs used in specimens 4A and 4D are same, maximum load of specimen 4D is twice larger than that of the control beam and even 1.6 times

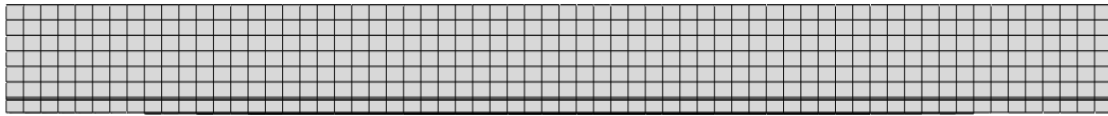


Fig. 4 Generated FE model

Table 4 Element types and materials model

Part	Element type	Material model	Elastic modulus
Concrete	3D continuum brick	Elastic and Concrete Damaged Plasticity	22 GPa
Steel reinforcement	3D Truss	Elastic and Plastic	190 GPa
Epoxy	Cohesive	Elastic Traction	2.46 GPa
CFRPs	Shell	Elastic	245.2 GPa

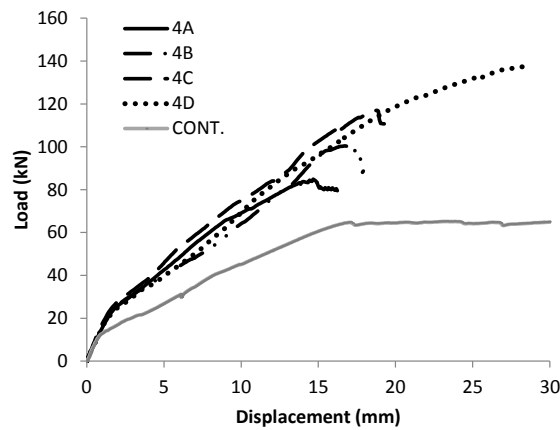


Fig. 5 Load-deflection curves of the tested beams

Table 5 Experimental results

Specimen	Max. Load (kN)	Max. load / total length of CFRP (kN/m)	Mid-span deflection at max. load (mm)	Steel strain at max. load ( $10^{-3}$ )	CFRP strain at max. load ( $10^{-3}$ )	Concrete strain at max. load ( $10^{-3}$ )
4A	84	11.67	14	2.135	2.337	-1.136
4B	100	18.52	17	2.458	2.666	-1.232
4C	117	17.73	19	2.623	3.244	-1.521
4D	138	19.17	28	10.265	3.355	-2.093
CONT.	69	-	76	7.119	-	-1.219

larger than that of specimen 4A. This is because specimen 4D uses tapered CFRPs, and length of first CFRPs for specimen 4D is much larger than specimen 4A. Therefore, it can be said that load capacities of beams with tapered CFRPs are determined by length of first CFRP layer as well as total length of CFRP sheets. Detailed experimental results, such as maximum load, mid-span deflection, and strains of steel bars, CFRP, and concrete at beam failures, are listed in Table 5.

3.1.2 Interfacial shear stress

By adopting Hooke’s law with force equilibrium, an equation to calculate interfacial shear stress,  $\tau$ , is obtained as following (Camata *et al.* 2007).

$$\tau = t_f E_f \frac{d\varepsilon}{dx} \tag{2}$$

$E_f$ : elastic modulus of FRP sheets,  $t_f$ : thickness of FRP sheets,  $\varepsilon$ : strain of FRP sheets

In the equation,  $t_f$  and  $E_f$  denotes thickness and elastic modulus of FRP sheets, respectively. Also,  $d\varepsilon/dx$  can be calculated using strains measured from multiple gauges attached on the CFRPs along the beam length. Figs. 6(a)-(d) illustrate the interfacial shear stresses along the CFRP length of specimens 4A, 4B, 4C, and 4D at 50%, 70%, 90%, and 95% of the maximum load level ( $P_u$ ). Beyond 95% of the maximum load level, it is assumed that debonding is initiated at the end of FRP sheets and redistributions of interfacial shear stress occur along the CFRP sheets. Commonly, maximum interfacial shear stress is observed at the end of FRP sheets. The maximum

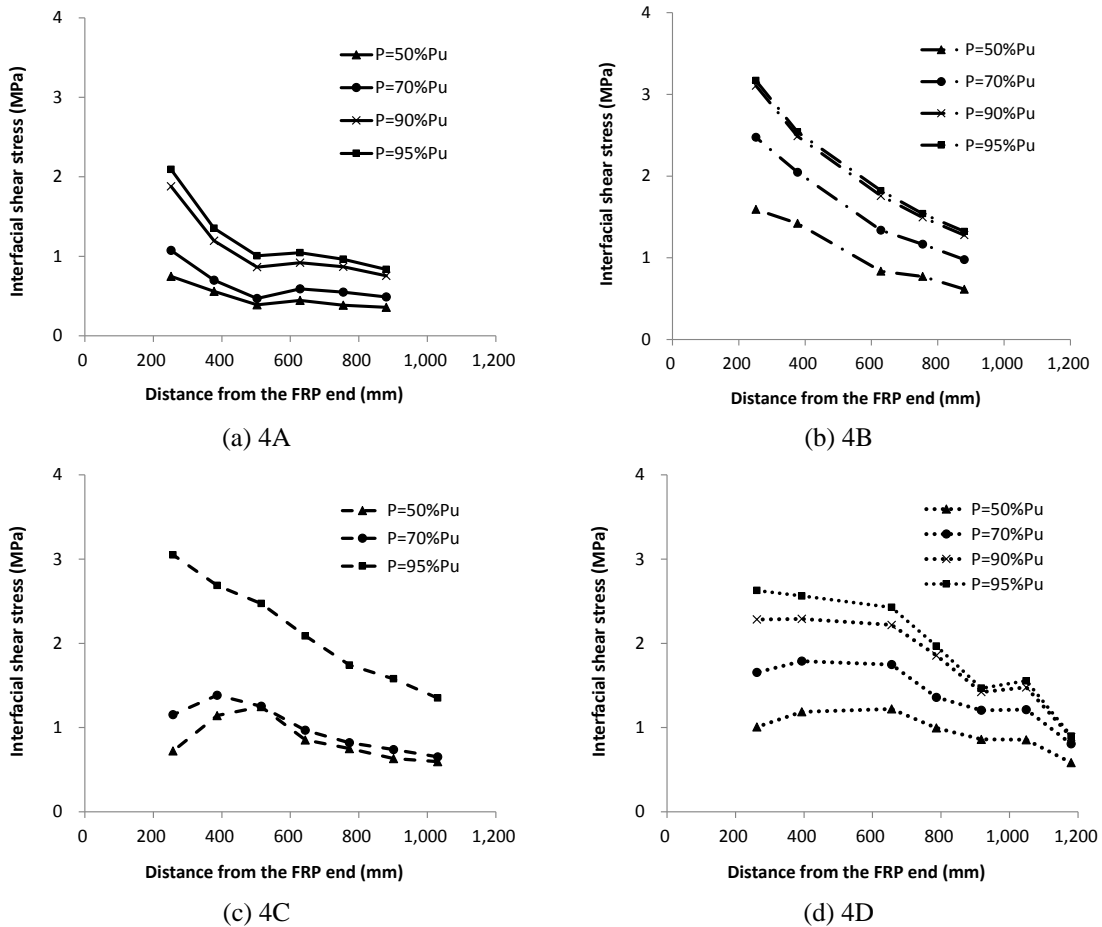


Fig. 6 Interfacial shear stress distributions at different load levels,  $P$

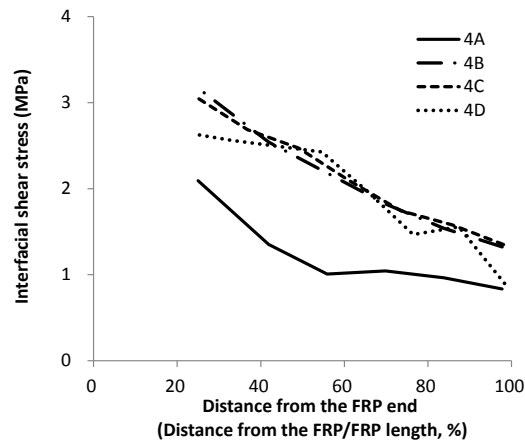


Fig. 7 Interfacial shear stress distributions at 95% of maximum load

interfacial shear stress value for specimen 4A is about 66-80% of the maximum interfacial shear stress values for specimens 4B, 4C, and 4D, which implies that debonding occurs in specimen 4A earlier than in the other specimens. Also for specimen 4A, the highest interfacial shear stress is about 1.6 times larger than the interfacial stress obtained at the next point. However, the highest interfacial shear stresses for specimens 4B, 4C, and 4D are about 1.02-1.24 times larger than the interfacial stress obtained at the next point. This means that interfacial shear stress is highly concentrated in the end of the CFRP sheets in specimen 4A, while the stresses in specimens 4B, 4C, and 4D are distributed evenly along the length of the CFRP sheets. In particular, for specimen 4D, less interfacial shear stress concentration is observed compared to the other specimens. Since the length of the first CFRP layer for specimens 4C and 4D are different from the lengths of the first CFRP layer for specimens 4A and 4B, interfacial stresses along the normalized distances from the CFRP end with length of first CFRP layer are illustrated in Fig. 7. The Fig. 7 shows that interfacial shear stress is not fully developed in 4A due to early debonding. Also, it is interesting to note that the interfacial shear stress distributions of specimens 4B, 4C, and 4D are smaller to each other at 95% of maximum loads.

### 3.1.3 Ductility

In this section, the ductility of RC beams strengthened with CFRPs is presented, because significant reduction of ductility is often reported for RC beams strengthened with FRPs and causes sudden failure of the beam in a brittle manner. Since it is difficult to find a unified definition of ductility, this study uses two different methods to present the deflection ductility,  $\mu_D$ , and energy ductility,  $\mu_E$ . The former is calculated from the ratio of midspan deflection at peak load to midspan deflection at yield of the steel reinforcements, and the latter is calculated from the ratio of midspan deflection at 75% of post-peak load to midspan deflection at yield of the steel reinforcements. Table 6 shows that the energy ductility is higher than the deflection ductility for all specimens. Also, the ductility of the RC beam without CFRP is higher than those of the RC beams with CFRPs as expected. Among the RC beams with CFRPs, specimen 4A shows lower ductility compared to specimens 4B, 4C, and 4D, which indicates the improvement of ductility by using tapered CFRPs for strengthening the RC beams. Even though the ductility of specimen 4D is about 50% of the control specimen, it is about 2-3 times larger than that of specimen 4A.

Table 6 Ductility of specimens

Specimen	Deflection ductility		Energy ductility	
	$\mu_D$	Ratio to CONT	$\mu_E$	Ratio to CONT
CONT	4.98	1.0	8.16	1.0
4A	1.11	0.22	1.16	0.14
4B	1.33	0.27	1.70	0.21
4C	1.43	0.29	1.85	0.23
4D	2.44	0.49	4.22	0.52

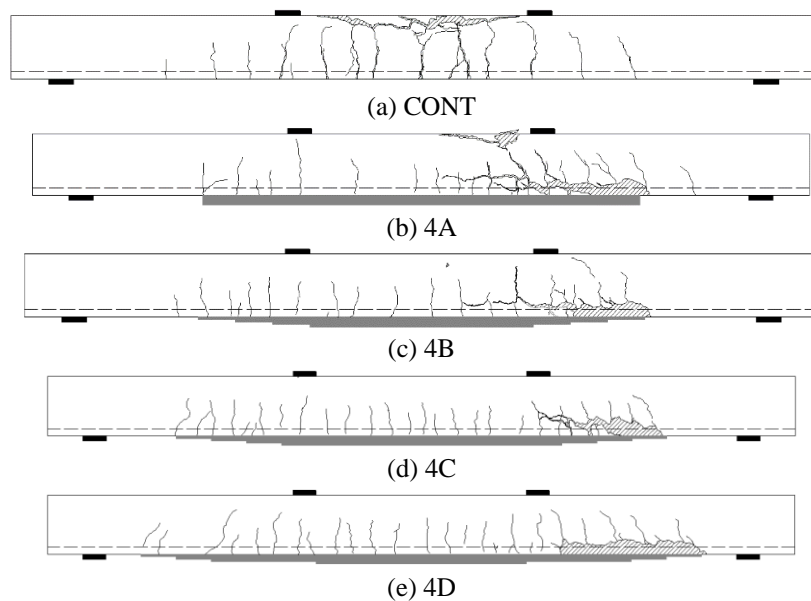


Fig. 8 Crack configurations and failure modes of specimens

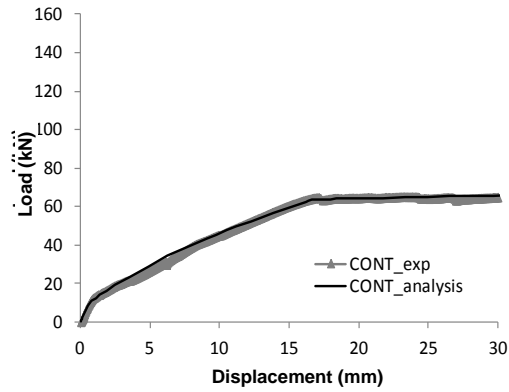
### 3.1.4 Failure modes

Crack configurations of the tested specimens after the loading tests are illustrated in Figs. 8(a)-(e). Hatched areas in the figures present locations where concrete is broken off from the main part of the specimens at failure. As shown in Fig. 8(a), CONT specimen shows flexural cracks and failure in the concrete compressive zone, while concrete separation due to the debonding of CFRPs is observed from the RC beams strengthened with CFRPs. For specimen 4A, a large crack is developed from CFRP debonding and propagates toward the concrete compressive zone. Compared to specimens 4A and 4B, specimens 4C and 4D show relatively smaller crack intervals and larger debonding areas, because the maximum loads at failure of specimens 4C and 4D are larger than those of specimens 4A and 4B.

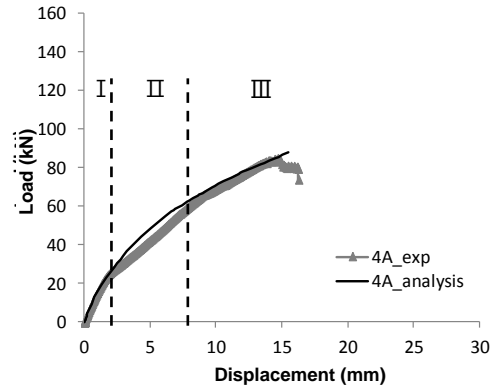
## 3.2 Analytical results

### 3.2.1 Load-deflection relationships

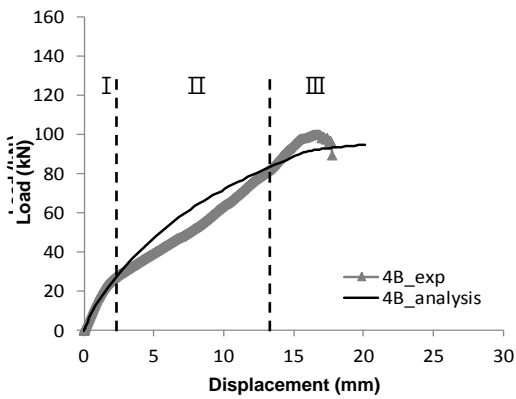
Analytical results of the load-deflection curves compared to the experimental results are



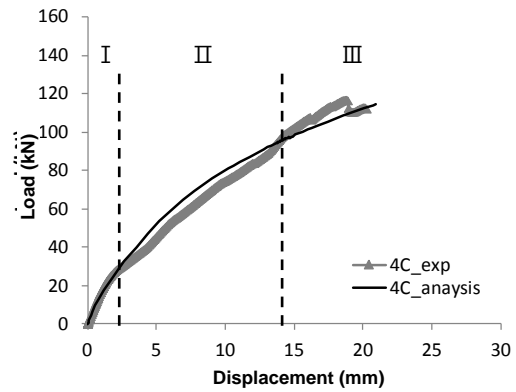
(a) CONT



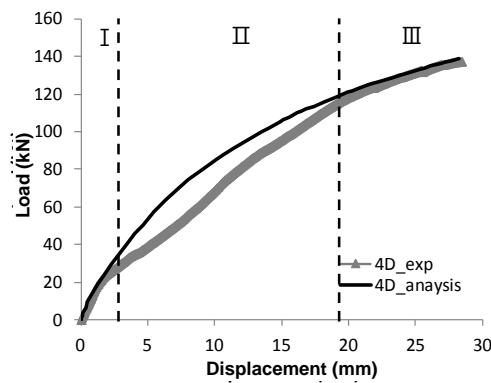
(b) 4A



(c) 4B



(d) 4C



(e) 4D

Fig. 9 Analytical and experimental results of load-deflection curves

presented in Figs. 9(a)-(e). Overall, the analytical and experimental results are in good agreement. In particular, Fig. 9(a) shows that elastic and plastic behaviors of the control beam are well

captured from the FE model. For the specimens 4A, 4B, 4C, and 4D, even though the CFRPs are modeled with same axial stiffness (elastic modulus $\times$ thickness of CFRPs), predictions from the FE models are well matched with experimental data, because debonding is considered in the cohesive zone model. In detail, there are certain regions of load-deflection curves where experimental and analytical results show different slopes. In order to explain this, the load-deflection curves obtained from experiments can be divided into three regions according to the slopes. The reason for slope change in the experiments may be because the contribution of the concrete, steel bars, and CFRPs to structural behavior changes according to stress status. For example, CFRP and steel bars play a major role of reinforcement in region II after concrete reaches its tensile limit, then CFRP sheets take place in region III after the steel bars are yielded. While the slopes of load-deflection curves obtained from experiments show relatively sudden changes, the analytical results show that slopes of load-deflection curves decrease constantly as the load increases.

### 2.2.2 Stress contours

Maximum principal stress contours on the side surface of RC beams at maximum loads are predicted from FE models as shown in Figs. 10(a)-(d). Commonly, high stresses can be found from the area near by CFRP sheet ends. Compared with specimens 4A, 4B, and 4C, the less stress concentrations in the lower area are seen in specimen 4D. These are because length of first CFRP layer of specimen 4D is longer than that of other specimens. Also, stresses are relatively evenly distributed along the length of CFRP sheets in specimen 4D due to large difference in length between CFRP layers. In order to compare stresses on adhesive layer among specimens at same load level, principal stress contours of epoxy at load of 92kN are illustrated in Figs. 11(a)-(d). For all specimens, stress concentration is observed from the end of epoxy layer, where debonding of

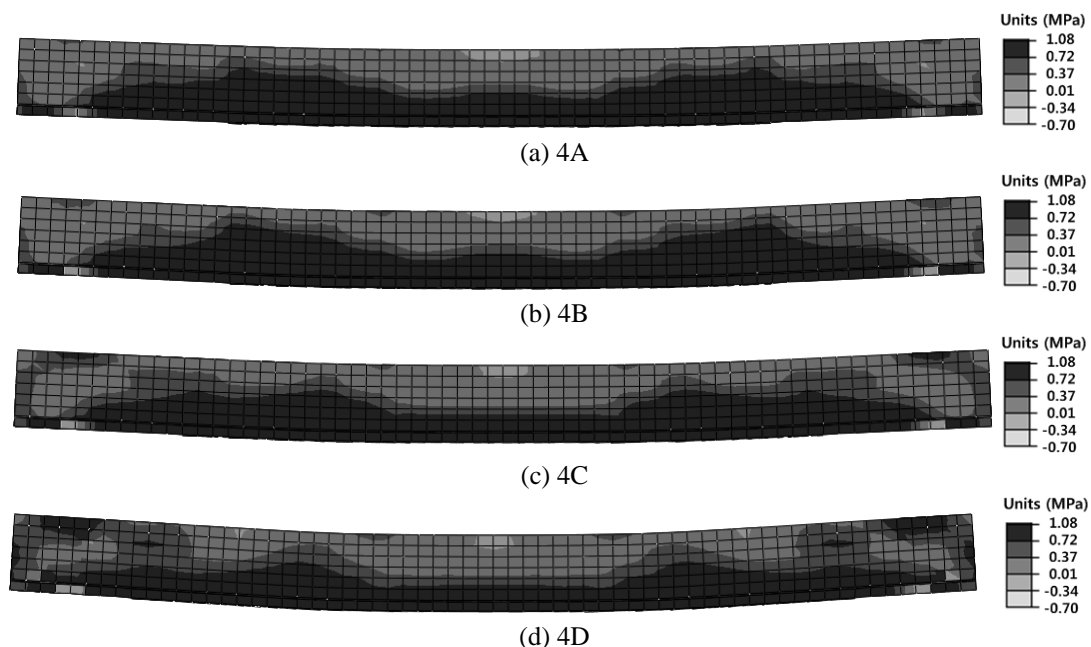


Fig. 10 Maximum principal stress contours with deformed configurations captured from side surface of FE models

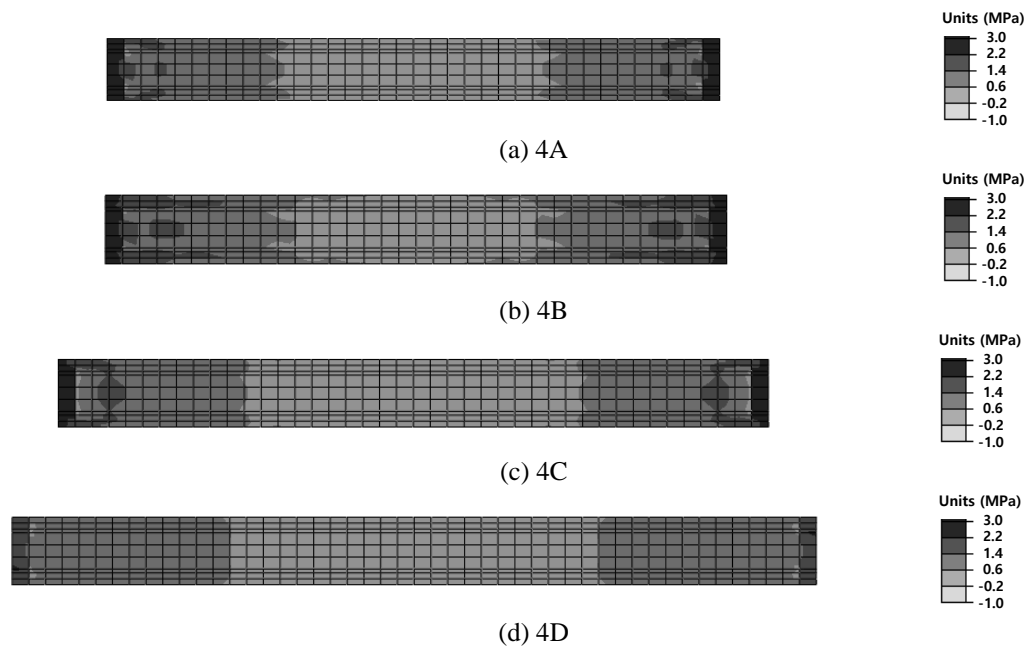


Fig. 11 Maximum principal stress contours with deformed configurations captured from side surface of FE models

CFRP sheets is initiated. Epoxy of specimen 4D shows lower stress distributions compared to other specimens, which confirms that debonding initiation is delayed in specimen 4D.

#### 4. Conclusions

This paper includes experimental and analytical studies to investigate structural and mechanical behaviors of RC beams strengthened with tapered CFRPs. Overall structural behaviors such as load-deflection relations, ductility, and interfacial shear stresses are obtained from experiments. Using FE analytical method, it is able to examine stress distributions of different material components and support experimental findings. From the experimental and analytical studies, conclusions can be summarized as follows.

(1) When RC beams are strengthened with four layers of CFRPs having the same length, beam failure due to debonding of CFRP layers occurs in the early stage of loading and ductility is significantly decreased compared to RC beam without CFRP reinforcement.

(2) Compared to the case of using non-tapered CFRPs, tapered CFRP is able to increase maximum load capacity and ductility of RC beams by 16-54% and 20-120%, respectively.

(3) Among the RC beams with tapered CFRPs, the better strengthening effect can be expected when length of the first CFRP layer directly attached to the RC beam increases. The reason for increase in maximum load capacity and ductility of RC beams with tapered CFRPs is that tapered CFRP sheets are able to delay debonding initiation caused by high stress concentrations occurred at the ends of CFRP sheets.

(4) The FE modeling approaches capture structural behaviors of the RC beams strengthened

using CFRP sheets with high accuracy by considering nonlinear material behaviors for steel, concrete, CFRP and epoxy. Especially, cohesive elements allow to simulate debonding initiation of adhesive layer.

(5) Stress contours obtained from the FE analyses show that high stress concentrations occur in the ends of CFRP sheets. However, tapered CFRP sheets with relatively large difference in length of each CFRP layer are able to reduce such stress concentrations.

## Acknowledgements

This research was supported by Basic Science Research Program through the National Research Foundation of Korea (NRF) funded by the Ministry of Education, Science and Technology (NRF-2011-0008824).

## References

- ABAQUS (2010), Theory Manual Version 6.10-3, Dassault Systems Simulia Corp., Providence, RI, USA.
- ACI committee 440 (2008), Guide for the Design and Construction of Externally Bonded FRP Systems for Strengthening Concrete Structures, American Concrete Institute, ACI 440, 2R-08.
- Al-Tamimi, A., Hawileh, R., Abdalla, J.A. and Rasheed, H. (2011), "Effects of ratio of CFRP plate length to shear span and end anchorage on flexural behavior of SCC R/C beams", *J. Compos. Constr.*, ASCE, **15**(6), 908-919.
- Brena, S.F. and Marcri, B.M. (2004), "Effect of carbon-fiber-reinforced polymer laminate configuration on the behavior of strengthened reinforced concrete beams", *J. Compos. Constr.*, ASCE, **8**(3), 229-240.
- Camata, G., Spacone, E. and Zarnic, R. (2007), "Experimental and nonlinear finite element studies of RC beams strengthened with FRP plates", *Compos. Part B*, **38**, 277-288.
- Choi, E.S., Utui, N. and Kim, H.S. (2013), "Experimental and analytical investigations on debonding of hybrid FRPs for flexural strengthening of RC beams", *Compos. Part B*, **45**(1), 248-256.
- Gao, B., Kim, J.K. and Leung, C.K.Y. (2006), "Effect of tapered FRP sheets on interlaminar fracture behavior of FRP concrete interface", *Compos. Part A*, **37**(10), 1605-1612.
- Hawileh, R., Naser, M. and Abdalla, J.A. (2013), "Finite Element Simulation of Reinforced Concrete Beams Externally Strengthened with Short-Length CFRP Plates", *Compos. Part B*, **45**(1), 1722-1730.
- Kang, T.H.K., Howell, J., Kim, S. and Lee, D.J. (2012), "A State-of-the-Art review on debonding failures of FRP laminates externally adhered to concrete", *Int. J. Concrete Struct. Mater.*, **6**(2), 123-134.
- Kim, H.S. and Shin, Y.S. (2011), "Flexural behavior of RC (RC) beams retrofitted with hybrid fiber reinforced polymers (FRPs) under sustaining loads", *Compos. Struct.*, **93**(2), 802-811.
- Kadhim, M.M.A. (2011), "Effect of CFRP sheet length on the behavior of HSC continuous Beam", *J. Therm. Compos. Mater.*, **25**(1), 33-44.
- Leung, C.K.Y. (2006), "FRP debonding from a concrete substrate: Some recent findings against conventional belief", *Cement Concrete Compos.*, **2**, 742-748.
- Maalej, M. and Leung, K.S. (2005), "Effect of beam size and FRP thickness on interfacial shear stress concentration and failure mode of FRP-strengthened beams", *Compos. Sci. Tech.*, **65**(7-8), 1148-1158.
- Mongi, B.O., Abdeldjelil, B. and Bae, S.W. (2009), "Effective bond length of FRP sheets externally bonded to concrete", *Int. J. Concrete Struct. Mater.*, **3**(2), 127-131.
- Obaidat, Y., Heyden, S. and Dahlblom, O. (2010), "The effect of CFRP and CFRP/Concrete interface models when modelling retrofitted RC beams with FEM", *Compos. Struct.*, **92**(6), 1391-1398.
- Smith, S.T. and Teng, J.G. (2002), "FRP-strengthened RC beams. II: assessment of debonding strength models", *Eng. Struct.*, **24**, 397-417.

- Teng, J.G., Yuan, H. and Chen, J.F. (2006), "FRP-to-concrete interfaces between two adjacent cracks: Theoretical model for debonding failure", *Int. J. Solid. Struct.*, **43**(18-19), 5750-5778.
- Teng, J.G., Chen, J.F., Smith, S.T. and Lam, L. (2011), *FRP Retrofitted RC Structures*, John Wiley & Sons, Inc.
- Yang, Q., Qin, Q. and Zheng, D. (2002), "Analytical and numerical investigation of interfacial stresses of FRP-concrete hybrid structure", *Compos. Struct.*, **57**(1-4), 221-226.

CC